Impact of Pilot Contamination Between Operators With Interfering Reconfigurable Intelligent Surfaces

Doğa Gürgünoğlu*, Emil Björnson*, Gábor Fodor*†
*KTH Royal Institute of Technology, Stockholm 100 44, Sweden
†Ericsson Research, Stockholm 164 80, Sweden

***Abstract*—In this paper, we study the impact of pilot contamination in a system where two operators serve their respective users with the assistance of two wide-band reconfigurable intelligent surfaces (RIS), each belonging to a single operator. We consider one active user per operator and they use disjoint narrow frequency bands. Although each RIS is dedicated to a single operator, both users' transmissions are reflected by both RISs. We show that this creates a new kind of pilot contamination effect when pilots are transmitted simultaneously. Since combating inter-operator pilot contamination in RIS-assisted networks would require long pilot signal sequences to maintain orthogonality among the users of different operators, we propose the orthogonal configurations of the RISs. Numerical results show that this approach completely eliminates pilot contamination, and significantly improves the performance in terms of channel estimation and equalization by removing the channel estimation bias.**

***Index Terms*—Reconfigurable intelligent surface, channel estimation, pilot contamination.**

I. Introduction

Pilot contamination is a key problem that frequently arises in wireless communication systems [1]. When multiple users use the same pilot sequences simultaneously in the same band, due to the limited channel coherence time, the base station (BS) cannot distinguish their channels, which typically results in poor channel estimates and extra beamformed interference towards pilot-sharing user equipments (UEs). Therefore, pilot contamination adversely affects the coherent reception of data, and methods to mitigate pilot contamination have been widely studied in the communication literature [1]–[4].

In recent years, reconfigurable intelligent surfaces (RISs) have arisen as a new technology component for 6G [5]. An RIS is a surface consisting of multiple reflecting elements that have sub-wavelength spacing and controllable reflection properties [6]. This feature provides partial control of the propagation environment that can lead to better services for users, especially when their serving BS is not in their line of sight (LOS). By adjusting the impedances of the individual elements via a RIS controller, the elements are capable of adding desired phase shifts to the reflected signals, thereby forming reflected beams in desired directions that can significantly boost the signal-to-interference-plus-noise ratio (SINR) at the receiver [5].

On the other hand, the addition of RISs to existing systems introduces new design and operational challenges. For example, the length of the pilot signal required by a single UE is proportional to the number of RIS elements (e.g., tens or hundreds), because the RIS must change its configuration to explore all channel dimensions [7], [8]. In addition, passive RIS causes multiplicative path losses, which increases the large-scale fading loss between the transmitter and the receiver [9]. Active RISs [10], on the other hand, are less energy efficient, and due to the presence of amplifiers, it introduces additional noise. While the aforementioned problems caused by the RIS have been recognized [11], pilot contamination caused by the presence of multiple RISs has not been studied in the literature. In this paper, however, we identify the creation of pilot contamination as another practical challenge: a UE that transmits pilots to its serving BS via multiple RIS, which change their configurations simultaneously, may cause a new kind of pilot contamination that has not been studied.

Wireless communication systems are governed by standards, and physical-layer specifications usually contain predefined sequences for pilot signals and codebooks for directional beamforming [12]. While the use RISs is not standardized yet, it is likely that the configuration sequences that facilitate the deployment of RISs while maintaining interoperability will be standardized. Consequently, when multiple cellular networks are deployed by different network operators in overlapping geographical areas, the RISs may adopt identical or overlapping pilot sequences and cause pilot contamination.

Due to the ability to change the environment's propagation characteristics, deploying multiple RISs in a geographical area also implies that pilot contamination can occur due to a UE's own pilot signal. Since this phenomenon may exacerbate the pilot contamination problem, it is clear that pilot contamination due to the presence of multiple RISs must be dealt with.

In this paper, we study the pilot contamination caused by the presence of multiple RISs by considering the uplink of a system consisting of two wide-band RISs, two single-antenna UEs, and two co-located single-antenna BSs, where the two UEs are subscribed to different operators with non-overlapping narrow-band channels at different frequencies. Each RIS is dedicated to a single operator, but both UE signals are reflected from both RISs. In this scenario, although there is no interference between the two UEs, both RISs affect both frequency bands. We propose the use of orthogonal RIS configuration sequences during pilot transmission to avoid pilot contamination. First, we describe the channel estimation procedure with a lack of information on channel statistics, i.e., when the channels are characterized by deterministic parameters. Assuming identical and orthogonal RIS configurations, we derive the statistics of the maximum likelihood (ML)

This study is supported by EU Horizon 2020 MSCA-ITN-METAWIRELESS, Grant Agreement 956256. E. Björnson was supported by FFL18-0277 grant from the Swedish Foundation for Strategic Research.

estimates and the effect of pilot contamination on channel estimation. Then we analyze how it affects the data estimation process, and discuss how this effect can be mitigated.

II. System Model

We consider the uplink of a cellular system consisting of two wide-band RIS, two single-antenna UE, and two co-located single-antenna BSs, as shown in Fig. 1, where each RIS has N reflecting elements. The two UEs are subscribed to different operators—who use site-sharing to reduce deployment costs—and transmit over two disjoint narrow frequency bands to their respective serving BSs. Each RIS is dedicated to and controlled by a single operator but affects both bands. We consider an environment where the direct UE-BS paths are blocked, while the UE-RIS and RIS-BS paths are operational. Since the BSs and RISs have fixed deployment locations, we assume the RIS-BS channels $\mathbf{h}_k$ are known, while the UE-RIS channels $\mathbf{g}_k$ are unknown and to be estimated for $k = 1, 2$.

The signal transmitted by UE k reaches its serving BS through the channels $\mathbf{h}_k$ and $\mathbf{g}_k$, for $k = 1, 2$. Importantly, the UEs' transmitted signals are also reflected by the non-serving operator's RISs towards their serving BSs, which contaminates the pilot signal reflected by the serving RIS. This phenomenon is illustrated in Fig. 1, where the resulting UE-RIS and RIS-BS channels are denoted by $\mathbf{p}_k$ and $\mathbf{q}_k$, respectively, for $k = 1, 2$.

Since the BSs are unaware of the channels $\mathbf{q}_k$ and $\mathbf{p}_k$, they adopt misspecified system models for the received pilot and data signals. We also assume that the prior distributions of the channels are unavailable. Consequently, the BSs estimate the channels $\mathbf{g}_1$ and $\mathbf{g}_2$ via classical non-Bayesian parameter estimation methods during the channel estimation phase and use the channel estimates to perform data estimation [13, Section IV.C] during the data transmission phase. Defining the pilot signal of UE k as $s_k \in \mathbb{C}$, the received pilot signals on bands 1 and 2 at the BSs can be expressed as

$$y_{p1} = \sqrt{P_p}\mathbf{h}_1^T\mathbf{\Phi}_1\mathbf{g}_1 s_1 + \sqrt{P_p}\mathbf{q}_1^T\mathbf{\Phi}_2\mathbf{p}_1 s_1 + w_{p1}, \quad (1a)$$

$$y_{p2} = \sqrt{P_p}\mathbf{h}_2^T\mathbf{\Phi}_2\mathbf{g}_2 s_2 + \sqrt{P_p}\mathbf{q}_2^T\mathbf{\Phi}_1\mathbf{p}_2 s_2 + w_{p2}, \quad (1b)$$

where y_{pk} denotes the received pilot signal, $w_{pk} \sim \mathcal{CN}(0, 1)$ denotes the receiver noise for band k, and $\mathbf{\Phi}_k = \text{diag}(e^{-j\phi_{k1}}, \ldots, e^{-j\phi_{kN}})$ denotes the kth RIS's response matrix. We assume $s_1 = s_2 = 1$ without loss of generality. For channel estimation, it is more convenient to rewrite (3) as

$$y_{p1} = \sqrt{P_p}\boldsymbol{\phi}_1^T\mathbf{D}_{\mathbf{h}_1}\mathbf{g}_1 + \sqrt{P_p}\boldsymbol{\phi}_2^T\mathbf{D}_{\mathbf{q}_1}\mathbf{p}_1 + w_{p1}, \quad (2a)$$

$$y_{p2} = \sqrt{P_p}\boldsymbol{\phi}_2^T\mathbf{D}_{\mathbf{h}_2}\mathbf{g}_2 + \sqrt{P_p}\boldsymbol{\phi}_1^T\mathbf{D}_{\mathbf{q}_2}\mathbf{p}_2 + w_{p2}, \quad (2b)$$

where $\mathbf{D}_{\mathbf{h}_k}$ and $\mathbf{D}_{\mathbf{q}_k}$ represent the diagonal matrices containing the elements of $\mathbf{h}_k$ and $\mathbf{q}_k$, and $\boldsymbol{\phi}_k$ denotes the column vectors containing the diagonal entries of $\mathbf{\Phi}_k$ for $k = 1, 2$.

As there are N parameters in $\mathbf{g}_1$ and $\mathbf{g}_2$, at least N linearly independent observations are needed to estimate them. To this end, we perform $L \geq N$ pilot transmissions over time, and we vertically stack the received pilot signals to obtain

$$\mathbf{y}_{p1} = \sqrt{P_p}\mathbf{B}_1\mathbf{D}_{\mathbf{h}_1}\mathbf{g}_1 + \sqrt{P_p}\mathbf{B}_2\mathbf{D}_{\mathbf{q}_1}\mathbf{p}_1 + \mathbf{w}_{p1}, \quad (3a)$$

$$\mathbf{y}_{p2} = \sqrt{P_p}\mathbf{B}_2\mathbf{D}_{\mathbf{h}_2}\mathbf{g}_2 + \sqrt{P_p}\mathbf{B}_1\mathbf{D}_{\mathbf{q}_2}\mathbf{p}_2 + \mathbf{w}_{p2}, \quad (3b)$$

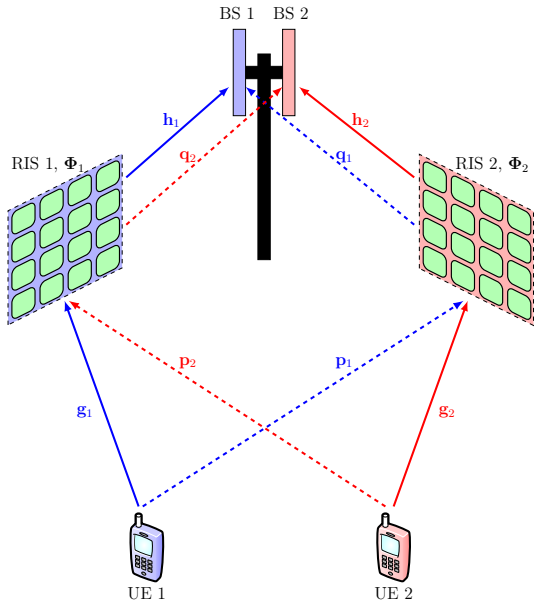

Fig. 1: System setup with two UEs, two RISs and two co-located single-antenna BSs. The blue channels correspond to frequency band 1, and the red channels correspond to frequency band 2, subscribed by UEs 1 and 2, respectively. Desired channels are denoted by solid lines, while the undesired channels whose existence are unknown to the BSs are denoted by dashed lines. Each channel vector is N-dimensional in line with the number of elements in each RIS.

where $\mathbf{y}_{pk} = [y_{pk}[1], \ldots, y_{pk}[L]]^T$ denotes the sequence of received uplink pilots from the kth UE over L time instances, and the matrices $\mathbf{B}_1$ and $\mathbf{B}_2$ represent the sequence of RIS configurations over L time instances, that is, $\mathbf{B}_k \triangleq [\boldsymbol{\phi}_k[1] \quad \ldots \quad \boldsymbol{\phi}_k[L]]^T$ for $k = 1, 2$. Recall that BS 1 is not aware of the reflection of UE 1's signal from RIS 2 and vice versa. Consequently, the BSs assumes the following misspecified received pilot signal models:

$$\hat{\mathbf{y}}_{p1} = \sqrt{P_p}\mathbf{B}_1\mathbf{D}_{\mathbf{h}_1}\mathbf{g}_1 + \mathbf{w}_{p1}, \quad (4a)$$

$$\hat{\mathbf{y}}_{p2} = \sqrt{P_p}\mathbf{B}_2\mathbf{D}_{\mathbf{h}_2}\mathbf{g}_2 + \mathbf{w}_{p2}. \quad (4b)$$

Based on (4), the estimation of $\mathbf{g}_1$ and $\mathbf{g}_2$ is described and analyzed in the next section.

III. Maximum Likelihood Channel Estimation

To estimate $\mathbf{g}_k$, which is N-dimensional, BS k requires at least N independent observations for $k = 1, 2$. Hence, both $\mathbf{B}_1, \mathbf{B}_2 \in \mathbb{C}^{L\times N}$ must have full column rank. Furthermore, we require that the RIS configurations on different time instances be orthogonal and contain entries on the unit circle that can be realized using a reflecting element. These assumptions result in $\mathbf{B}_k^H\mathbf{B}_k = L\mathbf{I}_N$. In classical non-Bayesian parameter estimation, the ML estimator is widely used, which maximizes the likelihood function of the received observation over the unknown parameter. Since the BSs have misspecified received pilot signal models, they will instead maximize the likelihood functions obtained from the misspecified model,

leading to misspecified maximum likelihood (MML) estimators. For (4), the MML estimator can be expressed as

$$\begin{aligned}\hat{\mathbf{g}}_k &= \arg\max_{\mathbf{g}_k} f(\mathbf{y}_{pk};\mathbf{g}_k)\\ &= \arg\max_{\mathbf{g}_k} \frac{1}{(\pi\sigma_w^2)^L}\exp\left(-\frac{\|\mathbf{y}_{pk}-\sqrt{P_p}\mathbf{B}_k\mathbf{D}_{\mathbf{h}_k}\mathbf{g}_k\|^2}{\sigma_w^2}\right)\\ &= \arg\min_{\mathbf{g}_k}\left\|\mathbf{y}_{pk}-\sqrt{P_p}\mathbf{B}_k\mathbf{D}_{\mathbf{h}_k}\mathbf{g}_k\right\|^2\\ &= \frac{1}{\sqrt{P_p}}\mathbf{D}_{\mathbf{h}_k}^{-1}(\mathbf{B}_k^H\mathbf{B}_k)^{-1}\mathbf{B}_k^H\mathbf{y}_{pk}\\ &= \frac{1}{L\sqrt{P_p}}\mathbf{D}_{\mathbf{h}_k}^{-1}\mathbf{B}_k^H\mathbf{y}_{pk}. \end{aligned} \tag{5}$$

In the following subsections, we describe the behavior of this estimator for two different choices of the $\mathbf{B}_k$ matrices.

A. Case 1: The RISs Adopt the Same Configuration Sequence

We discussed earlier that in the absence of inter-operator cooperation, it is highly likely that the RISs will use the same sequence of configurations during the channel estimation phase, which corresponds to $\mathbf{B}_1 = \mathbf{B}_2 = \mathbf{B}$.[1] In this case, (5) becomes

$$\hat{\mathbf{g}}_k = \mathbf{g}_k + \mathbf{D}_{\mathbf{h}_k}^{-1}\mathbf{D}_{\mathbf{q}_k}\mathbf{p}_k + \frac{1}{L\sqrt{P_p}}\mathbf{D}_{\mathbf{h}_k}^{-1}\mathbf{B}^H\mathbf{w}_{pk}. \tag{6}$$

Since we consider the channels as deterministic parameters, we obtain the probability distribution

$$\hat{\mathbf{g}}_k \sim \mathcal{CN}\left(\mathbf{g}_k + \mathbf{D}_{\mathbf{h}_k}^{-1}\mathbf{D}_{\mathbf{q}_k}\mathbf{p}_k, \frac{\sigma_w^2}{LP_p}(\mathbf{D}_{\mathbf{h}_k}^H\mathbf{D}_{\mathbf{h}_k})^{-1}\right) \tag{7}$$

We notice that $\hat{\mathbf{g}}_k$ is biased; that is, $\mathbf{b}_k \triangleq \mathbb{E}[\hat{\mathbf{g}}_k - \mathbf{g}_k] = \mathbf{D}_{\mathbf{h}_k}^{-1}\mathbf{D}_{\mathbf{q}_k}\mathbf{p}_k \neq \mathbf{0}$. The estimator bias does not vanish when increasing P_p or L, and decreasing σ_w^2, hence, it is not asymptotically unbiased. This is a new instance of an extensively studied phenomenon in the massive multiple input multiple output (MIMO) literature: pilot contamination [1], [2]. Interestingly, the RISs cause pilot contamination even between two non-overlapping frequency bands, which has not been widely recognized in the literature so far.

B. Case 2: The RISs Adopt Different Configuration Sequences

In this subsection, we consider the generic case of $\mathbf{B}_1 \neq \mathbf{B}_2$. To motivate the proposed method for configuring $\mathbf{B}_1$ and $\mathbf{B}_2$, we first consider the case where the BSs are aware of the true signal model in (3), and therefore can estimate both $\mathbf{g}_k$ and $\mathbf{r}_k \triangleq \mathbf{D}_{\mathbf{q}_k}\mathbf{p}_\mathbf{k}$. The resulting system model can be expressed as

$$\mathbf{y}_{p1} = \sqrt{P}_p\begin{bmatrix}\mathbf{B}_1\mathbf{D}_{\mathbf{h}_1} & \mathbf{B}_2\end{bmatrix}\begin{bmatrix}\mathbf{g}_1\\ \mathbf{r}_1\end{bmatrix} + \mathbf{w}_{p1}, \tag{8a}$$

$$\mathbf{y}_{p2} = \sqrt{P}_p\begin{bmatrix}\mathbf{B}_2\mathbf{D}_{\mathbf{h}_2} & \mathbf{B}_1\end{bmatrix}\begin{bmatrix}\mathbf{g}_2\\ \mathbf{r}_2\end{bmatrix} + \mathbf{w}_{p2}. \tag{8b}$$

In (8), a known linear transformation is applied to the parameter vector of interest in the presence of additive noise. Consequently, the ML estimates for UE 1's unknown channels become

$$\begin{bmatrix}\hat{\mathbf{g}}_1\\ \hat{\mathbf{r}}_1\end{bmatrix} = \frac{1}{\sqrt{P_p}}\begin{bmatrix}L\mathbf{D}_{\mathbf{h}_1}^H\mathbf{D}_{\mathbf{h}_1} & \mathbf{D}_{\mathbf{h}_1}^H\mathbf{B}_1^H\mathbf{B}_2\\ \mathbf{B}_2^H\mathbf{B}_1\mathbf{D}_{\mathbf{h}_1} & L\mathbf{I}_N\end{bmatrix}^{-1}\begin{bmatrix}\mathbf{D}_{\mathbf{h}_1}^H\mathbf{B}_1^H\\ \mathbf{B}_2^H\end{bmatrix}\mathbf{y}_{p1}. \tag{9}$$

Note that in this case, the total dimension of the unknown parameter vector is $2N$, hence, at least $2N$ independent observations are required for the matrix inverse to exist. The structure in (9) applies to UE 2 with alternated indices, and it gives the ML estimator, which is both unbiased and efficient, since (8) is a linear observation model with additive Gaussian noise [14, Theorem 7.3]. Hence, (9) is unbiased irrespective of other parameters such as σ_w^2, L, P_p, and it achieves the Cramér-Rao Lower Bound (CRLB), which provides a lower bound on the mean squared error (MSE) of any unbiased estimator [13]. It has to be noted that when $\mathbf{B}_1^H\mathbf{B}_2 = \mathbf{0}$, (9) becomes

$$\begin{aligned}\begin{bmatrix}\hat{\mathbf{g}}_1\\ \hat{\mathbf{r}}_1\end{bmatrix} &= \frac{1}{L\sqrt{P_p}}\begin{bmatrix}\mathbf{D}_{\mathbf{h}_1}^H\mathbf{D}_{\mathbf{h}_1} & \mathbf{0}\\ \mathbf{0} & \mathbf{I}_N\end{bmatrix}^{-1}\begin{bmatrix}\mathbf{D}_{\mathbf{h}_1}^H\mathbf{B}_1^H\\ \mathbf{B}_2^H\end{bmatrix}\mathbf{y}_{p1}\\ &= \frac{1}{L\sqrt{P_p}}\begin{bmatrix}\mathbf{D}_{\mathbf{h}_1}^{-1}\mathbf{B}_1^H\\ \mathbf{B}_2^H\end{bmatrix}\mathbf{y}_{p1}. \end{aligned} \tag{10}$$

Note that the expression for $\hat{\mathbf{g}}_1$ in (10) is the same as in (5). This shows that when $\mathbf{B}_1^H\mathbf{B}_2 = \mathbf{0}$, the MML in (5) coincides with the ML estimator; that is, the misspecified model is sufficient when the configuration sequences are designed to alleviate pilot interference. The probability distribution of $\hat{\mathbf{g}}_k$ in this case can be expressed as

$$\hat{\mathbf{g}}_k \sim \mathcal{CN}\left(\mathbf{g}_k, \frac{\sigma_w^2}{LP_p}(\mathbf{D}_{\mathbf{h}_k}^H\mathbf{D}_{\mathbf{h}_k})^{-1}\right), \tag{11}$$

which shows that choosing the RIS configuration sequences such that $\mathbf{B}_1$ and $\mathbf{B}_2$ removes the bias from the MML estimator. However, the major setback of this approach is that the minimum number of observations required for this channel estimation procedure is $2N$ instead of N, due to the fact that the $2N$-many L-dimensional columns must all be orthogonal to each other, for which $L \geq 2N$ is required. Considering that the estimator bias in (7) does not vanish with increasing L, this is a necessary sacrifice. Hence, it has to be noted that the number of pilot transmissions increases linearly with the number of RISs deployed in proximity. In the next section, data signal transmission and its estimation will be analyzed.

C. MSE During Channel Estimation

We consider the MSE as the channel estimation performance metric, which is the trace of the error covariance matrix that is derived in this section. In this derivation, we do not assume a particular choice of $\mathbf{B}_1, \mathbf{B}_2$, but we utilize the basic assumption $\mathbf{B}_k\mathbf{B}_k^H = L\mathbf{I}_N$. Consequently, we use $\mathbf{b}_k$ to denote the potential estimator bias. We can then compute the error covariance matrix as

$$\begin{aligned}\mathbf{\Sigma}_{e,k} &= \mathbb{E}\left[(\hat{\mathbf{g}}_k - \mathbf{g}_k)(\hat{\mathbf{g}}_k - \mathbf{g}_k)^H\right]\\ &= \mathbf{b}_k\mathbf{b}_k^H + \frac{1}{LP_p}\mathbb{E}\left[\mathbf{D}_{\mathbf{h}_k}^{-1}\mathbf{w}_{pk}\mathbf{w}_{pk}^H\mathbf{D}_{\mathbf{h}_k}^{-H}\right]\\ &= \mathbf{b}_k\mathbf{b}_k^H + \frac{\sigma_w^2}{LP_p}\left(\mathbf{D}_{\mathbf{h}_k}\mathbf{D}_{\mathbf{h}_k}^H\right)^{-1}. \end{aligned} \tag{12}$$

[1]The analysis in this paper can be easily extended to the case when $\mathbf{B}_1 = \mathbf{U}\mathbf{B}_2$ for some unitary matrix $\mathbf{U}$, so that configuration sequences have identical spans. It is the overlap of the spans that can cause issues.

Consequently, the trace of the error covariance matrix becomes

$$\mathrm{tr}(\mathbf{\Sigma}_{e,k}) = \|\mathbf{b}_k\|^2 + \frac{\sigma_w^2}{LP_p}\sum_{n=1}^{N}\frac{1}{|h_{kn}|^2} \tag{13}$$

Note that for high P_p, L, and low σ_w^2, the second term in (13) vanishes, and the trace of the error covariance converges to $\|\mathbf{b}_k\|^2$ which depend on the configuration of $\mathbf{B}_1, \mathbf{B}_2$:

$$\|\mathbf{b}_k\|^2 = \begin{cases} \sum_{n=1}^{N}\frac{|r_{kn}|^2}{|h_{kn}|^2} & \mathbf{B}_1 = \mathbf{B}_2, \\ 0 & \mathbf{B}_1^H\mathbf{B}_2 = \mathbf{0}. \end{cases} \tag{14}$$

This result shows that configuring the RISs such that $\mathbf{B}_1^H\mathbf{B}_2 = \mathbf{0}$ removes the asymptotic floor on the average MSE, which comes from the energy of the estimator bias. On the other hand, when the intended RIS-BS links $\mathbf{h}_1, \mathbf{h}_2$ are strong relative to the unintended and unknown overall link $\mathbf{r}_k$, the estimator bias will be weaker and the cost of choosing $\mathbf{B}_1 = \mathbf{B}_2$ will be lower. Nevertheless, pilot contamination results in a fundamental error floor, even if the RISs are utilized in different bands. In the next section, we consider the estimation of data based on the channel estimation performed in this section and analyze the consequence of pilot contamination in this phase.

IV. Data Transmission

The channel estimation is followed by data transmission. We consider a data packet with a duration shorter than the channel coherence time, therefore, the channels acting on the transmitted data signals are the same as in the channel estimation part. Defining the data signal transmitted by the kth UE as $x_k \sim \mathcal{CN}(0,1)$, we can express the received data as

$$y_1 = \sqrt{P_d}(\mathbf{h}_1^T\hat{\mathbf{\Phi}}_1\mathbf{g}_1 + \mathbf{q}_1^T\hat{\mathbf{\Phi}}_2\mathbf{p}_1)x_1 + w_1, \tag{15a}$$

$$y_2 = \sqrt{P_d}(\mathbf{h}_2^T\hat{\mathbf{\Phi}}_2\mathbf{g}_2 + \mathbf{q}_2^T\hat{\mathbf{\Phi}}_1\mathbf{p}_2)x_2 + w_2, \tag{15b}$$

where $w_k \sim \mathcal{CN}(0,\sigma_w^2)$ denotes the receiver noise, P_d denotes the data transmission power, and the RIS configuration matrices $\hat{\mathbf{\Phi}}_k$ are selected based on the estimated channels to maximize the average channel gain as shown in [8, Sec. II]:

$$\begin{aligned} &\hat{\phi}_{kn} = \arg(h_{kn}) + \arg(\hat{g}_{kn}), \\ &\hat{\mathbf{\Phi}}_k = \mathrm{diag}\left(e^{-j\hat{\phi}_{k1}}, \ldots, e^{-j\hat{\phi}_{kN}}\right). \end{aligned} \tag{16}$$

However, since the BSs are unaware of the unintended reflections and base their data estimation on channel estimates, they assume the following misspecified received data signal models:

$$\hat{y}_1 = \sqrt{P_d}\mathbf{h}_1^T\hat{\mathbf{\Phi}}_1\hat{\mathbf{g}}_1x_1 + w_1, \tag{17a}$$

$$\hat{y}_2 = \sqrt{P_d}\mathbf{h}_2^T\hat{\mathbf{\Phi}}_2\hat{\mathbf{g}}_2x_2 + w_2. \tag{17b}$$

Introducing the notation $m_k \triangleq \sqrt{P_d}(\mathbf{h}_k^T\hat{\mathbf{\Phi}}_k\mathbf{g}_k + \mathbf{q}_k^T\hat{\mathbf{\Phi}}_j\mathbf{p}_k)$ for $j,k \in \{1,2\}, j \neq k$, and $\hat{m}_k \triangleq \sqrt{P_d}\mathbf{h}_k^T\hat{\mathbf{\Phi}}_k\hat{\mathbf{g}}_k$, (15) and (17) can be expressed as

$$y_k = m_kx_k + w_k, \quad k = 1,2, \tag{18a}$$

$$\hat{y}_k = \hat{m}_kx_k + w_k, \quad k = 1,2. \tag{18b}$$

Based on the misspecified observation model in (18b), the BSs estimate x_k by using the misspecified minimum mean squared error (MMSE) estimator

$$\hat{x}_k = \frac{\hat{m}_k^*}{|\hat{m}_k|^2 + \sigma_w^2}y_k, \quad k = 1,2. \tag{19}$$

In this section, we consider the MSE between x_k and $\hat{x}_k$ as the performance metric for the data transmission. We derive the data estimation MSE for UE k as

$$\begin{aligned} &\mathbb{E}\left[|x_k - \hat{x}_k|^2\right] = 1 + \mathbb{E}\left[|\hat{x}_k|^2\right] - 2\mathrm{Re}(\mathbb{E}[x_k\hat{x}_k^*]) \\ &= 1 + \mathbb{E}\left[\frac{|\hat{m}_k|^2(|m_k|^2+\sigma_w^2)}{(|\hat{m}_k|^2+\sigma_w^2)^2}\right] \\ &- 2\mathrm{Re}\left(\mathbb{E}\left[\frac{\hat{m}_km_k^*}{|\hat{m}_k|^2+\sigma_w^2}\right]\right) \\ &= 1 + \mathbb{E}\left[\frac{|\hat{m}_k|^2(|m_k|^2+\sigma_w^2) - 2\mathrm{Re}(\hat{m}_1m_1^*)(|\hat{m}_k|^2+\sigma_w^2)}{(|\hat{m}_k|^2+\sigma_w^2)^2}\right] \\ &= 1 + \mathbb{E}\left[\frac{|\hat{m}_k|^2(|m_k|^2+\sigma_w^2) - 2\mathrm{Re}(\hat{m}_1m_1^*)(|\hat{m}_k|^2+\sigma_w^2)}{(|\hat{m}_k|^2+\sigma_w^2)^2}\right] \\ &+ \mathbb{E}\left[\frac{\sigma_w^2(|m_k|^2+\sigma_w^2) - \sigma_w^2(|m_k|^2+\sigma_w^2)}{(|\hat{m}_k|^2+\sigma_w^2)^2}\right] \\ &= 1 + \mathbb{E}\left[\frac{(|\hat{m}_k|^2+\sigma_w^2)(|m_k|^2+\sigma_w^2 - 2\mathrm{Re}(\hat{m}_km_k^*))}{(\hat{m}_k^2+\sigma_w^2)^2}\right] \\ &- \mathbb{E}\left[\frac{\sigma_w^2(|m_k|^2+\sigma_w^2)}{(\hat{m}_k^2+\sigma_w^2)^2}\right] \\ &= \mathbb{E}\left[\frac{|m_k-\hat{m}_k|^2+2\sigma_w^2}{|\hat{m}_k|^2+\sigma_w^2}\right] - \mathbb{E}\left[\frac{\sigma_w^2(|m_k|^2+\sigma_w^2)}{(|\hat{m}_k|^2+\sigma_w^2)^2}\right]. \end{aligned} \tag{20}$$

Defining $\epsilon_k \triangleq m_k - \hat{m}_k$, (20) can be rewritten as

$$\mathbb{E}[|x_k - \hat{x}_k|^2] = \mathbb{E}\left[\frac{|\epsilon_k|^2+2\sigma_w^2}{|m_k-\epsilon_k|^2+\sigma_w^2} - \frac{\sigma_w^2(|m_k|^2+\sigma_w^2)}{(|m_k-\epsilon_k|^2+\sigma_w^2)^2}\right] \tag{21}$$

To examine the impact of pilot contamination on the data estimation performance more clearly, we now consider channel estimation at high signal-to-noise ratios (SNRs), so that the estimation error only comes from the estimator bias, i.e., pilot contamination. This happens when L or P_p is high and/or σ_w^2 is low, which results in that the estimator covariances in (7) and (11) become zero. For notational convenience, we consider the case where P_p is arbitrarily large so that $\lim_{P_p\to\infty}\hat{\mathbf{g}}_k = \mathbf{g}_k + \mathbf{b}_k$, where

$$\mathbf{b}_k = \begin{cases} \mathbf{D}_{\mathbf{h}_k}^{-1}\mathbf{D}_{\mathbf{q}_k}\mathbf{p}_k & \mathbf{B}_1 = \mathbf{B}_2, \\ \mathbf{0} & \mathbf{B}_1^H\mathbf{B}_2 = \mathbf{0}. \end{cases} \tag{22}$$

A. Data MSE with Channel Estimation at High SNR

In (21), ϵ_k and m_k are functions of $\hat{\mathbf{g}}_1$ and $\hat{\mathbf{g}}_2$, therefore as $\hat{\mathbf{g}}_1$ and $\hat{\mathbf{g}}_2$ converge to their means, ϵ_k and m_k become

$$\overline{m}_k = \sqrt{P_d}(\mathbf{h}_k^T\bar{\mathbf{\Phi}}_k\mathbf{g}_k + \mathbf{q}_k^T\bar{\mathbf{\Phi}}_j\mathbf{p}_k), \tag{23a}$$

$$\bar{\epsilon}_k = \sqrt{P_d}(\mathbf{q}_k^T\bar{\mathbf{\Phi}}_j\mathbf{p}_k - \mathbf{h}_k^T\bar{\mathbf{\Phi}}_k\mathbf{b}_k), \tag{23b}$$

for $j,k \in \{1,2\}$ and $j \neq k$. $\bar{\mathbf{\Phi}}_k$ denotes the RIS configuration computed according to (16) with $\hat{\mathbf{g}}_k = \mathbf{g}_k + \mathbf{b}_k$.

At high SNR, the MSE in (21) can be rewritten as

$$\text{MSE} = \frac{|\bar{\epsilon}_k|^2 + 2\sigma_w^2}{|\overline{m}_k - \bar{\epsilon}_k|^2 + \sigma_w^2} - \frac{\sigma_w^2(|\overline{m}_k|^2 + \sigma_w^2)}{(|\overline{m}_k - \bar{\epsilon}_k|^2 + \sigma_w^2)^2}. \quad (24)$$

This is a practically achievable limit since RIS-aided systems require large pilot sequences over a narrow bandwidth, so the SNR might be larger than in the data transmission phase.

B. Data MSE with Transmission at High SNR

In the previous subsection, we obtained the expression for data MSE when the channels are estimated at a high pilot SNR, while the data transmission is done at an arbitrary SNR. To study the case when also the data transmission a step further, we let $\sigma_w^2 \to 0$, which results in the limit

$$\lim_{\sigma_w^2 \to 0} \text{MSE} = \frac{|\bar{\epsilon}_k|^2}{|\overline{m}_k - \bar{\epsilon}_k|^2}. \quad (25)$$

Note that the resulting expression denotes the ratio between the estimated overall single input single output (SISO) channel $\hat{m}_k$'s power and the mismatch parameter ϵ_k's power. Recall that $\mathbf{b}_k$ depends on which RIS pilot sequence is utilized. For $\mathbf{B}_1 = \mathbf{B}_2$, we can obtain ϵ_k as

$$\begin{aligned}
\epsilon_k &= \sqrt{P_d}\mathbf{q}_k^T\hat{\mathbf{\Phi}}_j\mathbf{p}_k - \sqrt{P_d}\mathbf{h}_k^T\hat{\mathbf{\Phi}}_k\mathbf{D}_{\mathbf{h}_1}^{-1}\mathbf{D}_{\mathbf{q}_1}\mathbf{p}_1 \\
&= \sqrt{P_d}\mathbf{q}_k^T\hat{\mathbf{\Phi}}_j\mathbf{p}_k - \sqrt{P_d}\hat{\phi}_k\mathbf{D}_{\mathbf{h}_k}\mathbf{D}_{\mathbf{h}_k}^{-1}\mathbf{D}_{\mathbf{q}_1}\mathbf{p}_1 \\
&= \sqrt{P_d}\mathbf{q}_k^T\hat{\mathbf{\Phi}}_j\mathbf{p}_k - \sqrt{P_d}\hat{\phi}_k\mathbf{D}_{\mathbf{q}_1}\mathbf{p}_1 \\
&= \sqrt{P_d}\mathbf{q}_k^T\hat{\mathbf{\Phi}}_j\mathbf{p}_k - \sqrt{P_d}\mathbf{q}_k^T\hat{\mathbf{\Phi}}_k\mathbf{p}_k \\
&= \sqrt{P_d}\mathbf{q}_k^T(\hat{\mathbf{\Phi}}_j - \hat{\mathbf{\Phi}}_k)\mathbf{p}_k. \quad (26)
\end{aligned}$$

On the other hand, $\mathbf{B}_1^H\mathbf{B}_2 = 0$ removes $\mathbf{b}_k$ for $k \in \{1, 2\}$. Consequently, we have

$$\epsilon_k = \begin{cases} \sqrt{P_d}\mathbf{q}_k^T(\hat{\mathbf{\Phi}}_j - \hat{\mathbf{\Phi}}_k)\mathbf{p}_k & \mathbf{B}_1 = \mathbf{B}_2, \\ \sqrt{P_d}\mathbf{q}_k^T\hat{\mathbf{\Phi}}_j\mathbf{p}_k & \mathbf{B}_1^H\mathbf{B}_2 = \mathbf{0}. \end{cases} \quad (27)$$

It is possible to observe that the ϵ_k corresponds to only the unintended reflection path itself when $\mathbf{B}_1^H\mathbf{B}_2 = \mathbf{0}$. On the other hand, $\mathbf{B}_1 = \mathbf{B}_2$ yields an expression depending on the difference between the two RISs' configurations during data transmission. Since each RIS is configured based on the channels of their respective users, it is highly unlikely that the configurations will be close. Moreover, it has to be noted that the RIS configuration of the non-serving RIS is different among the two cases since the channel estimates are also different.

V. Numerical Results

In this section, numerical results are provided to demonstrate the impact of pilot contamination in both the channel and data estimation phases. We consider $N = 256$ RIS elements. First, we demonstrate the results for the trace of the channel estimation error covariance matrix (i.e., the sum MSE). Then, for a single set of channel realizations, we provide the data estimation MSE for different data transmission powers. We also provide a Cumulative Distribution Function (CDF) plot for the high-SNR data estimation MSE floors under $\mathbf{B}_1 = \mathbf{B}_2$ and $\mathbf{B}_1^H\mathbf{B}_2 = \mathbf{0}$. The list of parameters used can be found in Table I.

TABLE I: Parameters used in the numerical results.

Parameter	Value
P_p or P_d	$-30, -25, \ldots, 40$ dBm^2
UE-RIS path loss	-80 dB
RIS-BS path loss	-60 dB
σ_w^2	-90 dBm
N	256
L	513

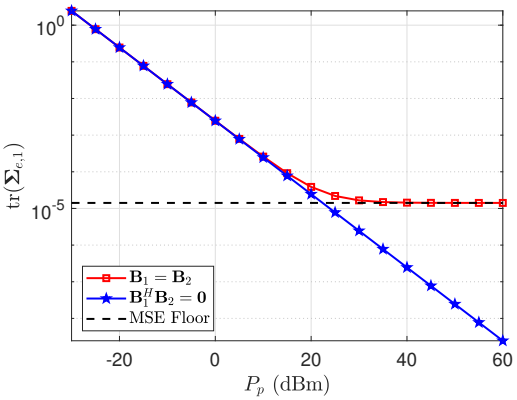

Fig. 2: Pilot transmission power versus channel estimation MSE.

A. Channel Estimation

For the channel estimation, we consider the MSE as our performance metric. Moreover, we consider the results for a single UE, since the results for different UEs only differ by the channel realizations. In Fig. 2, we plot (13) for different values of P_p, and we also provide the high-SNR floor for the case where $\mathbf{B}_1 = \mathbf{B}_2$. Note that at lower transmission powers, the covariance matrix of the estimator acts dominantly, hence, both RIS configurations perform nearly the same. However, after $P_p = 20$ dBm, the power of the estimator bias starts to dominate, and the average MSE for $\mathbf{B}_1 = \mathbf{B}_2$ goes to the floor denoted by the black dashed line, which is given by (14). On the other hand, the average MSE for $\mathbf{B}_1^H\mathbf{B}_2 = \mathbf{0}$ does not stop there but keeps decreasing towards zero. As mentioned before, the MML estimators used by the BSs coincide with the true ML estimators when the RISs are configured such that $\mathbf{B}_1^H\mathbf{B}_2 = \mathbf{0}$.

B. Data Estimation

In Fig. 3, the data estimation MSE performance with the two RIS pilot configurations are analyzed when the channel estimation SNR is high. That is, (24) is plotted for $\mathbf{B}_1 = \mathbf{B}_2$ and $\mathbf{B}_1^H\mathbf{B}_2 = \mathbf{0}$. In addition, the case where all of the channels are perfectly known is plotted to serve as the golden standard, labeled as *Perfect channel state information (CSI)*. However, even when all the channels are perfectly known, each RIS is assumed to be optimized according to the subscribed UE's CSI. Note that although the channel estimation SNR is high, $\mathbf{B}_1 = \mathbf{B}_2$ yields biased estimates of $\mathbf{g}_1$ due to pilot contamination caused by self-interference. On the other hand, $\mathbf{B}_1^H\mathbf{B}_2 = \mathbf{0}$ yields the true $\mathbf{g}_1$ as the estimate, however, since BS 1 is unaware of the path through

[2]The results for $P_p = 45, 50, 55,$ and 60 dBm are also demonstrated in Fig. 2 to display the high SNR floor more clearly.

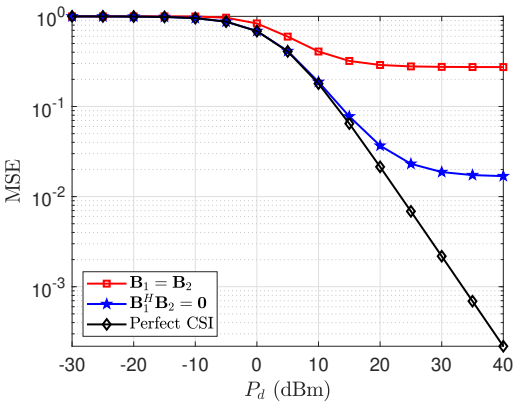

Fig. 3: Data transmission power versus data estimation MSE with high channel estimation SNR.

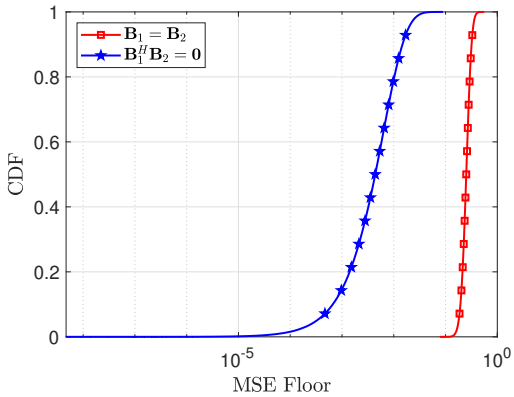

Fig. 4: CDF of the data-MSE floors for two RIS pilot configurations for i.i.d. Rayleigh fading.

the second RIS, the data estimate is biased, hence, there is still a high data transmission SNR floor. At around $P_d = 5$ dBm, $\mathbf{B}_1 = \mathbf{B}_2$ starts to approach the high-SNR floor. On the other hand, $\mathbf{B}_1^H\mathbf{B}_2 = \mathbf{0}$ does not suffer from the lack of awareness of the second RIS path until around $P_d = 20$ dBm. Hence, Fig. 3 clearly shows the benefit of configuring the RIS pilot configurations sequences orthogonally.

Note that (25) and (27) do not guarantee the superiority of $\mathbf{B}_1^H\mathbf{B}_2 = \mathbf{0}$ over $\mathbf{B}_1 = \mathbf{B}_2$, since if both RISs were configured identically during the data transmission phase, $\mathbf{B}_1 = \mathbf{B}_2$ would not suffer from a high-SNR data estimation MSE floor. To demonstrate that this scenario is highly unlikely, empirical CDFs of the MSE floors at high SNR are provided. We generate each channel according to $\mathcal{CN}(\mathbf{0}, \mathbf{I}_N)$, and then scale them according to the path losses given in Table I. The resulting CDFs are provided in Fig. 4. This figure is generated by using 10^6 different sets of channel realizations for $N = 32$ RIS elements. With a probability less then 10^{-6}, the high-SNR floor under $\mathbf{B}_1^H\mathbf{B}_2 = \mathbf{0}$ is much lower than that of $\mathbf{B}_1 = \mathbf{B}_2$, clearly demonstrating the benefit of using orthogonal RIS pilot configurations over identical configurations.

VI. Conclusions

In this paper, we have studied the impact of pilot contamination in a system consisting of two wide-band RISs, two single-antenna UEs, and two co-located single-antenna BSs. We have demonstrated that the presence of multiple RISs in the same area causes pilot contamination, although the UEs are subscribed to different operators and transmit over disjoint narrow frequency bands. To combat this new type of pilot contamination, we proposed the use of orthogonal RIS configurations during pilot transmission. In the numerical results, we have clearly shown that the proposed approach eliminates pilot contamination completely, and decreases data estimation MSE significantly. While increasing the number of pilots to configure RISs orthogonally alleviates pilot contamination, more efficient ways of dealing with this problem are needed in the future.

References

[1] T. L. Marzetta, "Noncooperative cellular wireless with unlimited numbers of base station antennas," *IEEE Trans. Wireless Commun.*, vol. 9, no. 11, pp. 3590–3600, 2010.

[2] L. Sanguinetti, E. Björnson, and J. Hoydis, "Toward Massive MIMO 2.0: Understanding spatial correlation, interference suppression, and pilot contamination," *IEEE Trans. Commun.*, vol. 68, no. 1, 2020.

[3] J. Jose, A. Ashikhmin, T. L. Marzetta, and S. Vishwanath, "Pilot contamination and precoding in multi-cell TDD systems," *IEEE Trans. Wireless Commun.*, vol. 10, no. 8, pp. 2640–2651, 2011.

[4] V. Saxena, G. Fodor, and E. Karipidis, "Mitigating pilot contamination by pilot reuse and power control schemes for massive MIMO systems," in *2015 IEEE 81st Vehicular Technology Conference (VTC Spring)*, 2015, pp. 1–6.

[5] C. Pan, H. Ren, K. Wang, J. F. Kolb, M. Elkashlan, M. Chen, M. Di Renzo, Y. Hao, J. Wang, A. L. Swindlehurst, X. You, and L. Hanzo, "Reconfigurable intelligent surfaces for 6G systems: Principles, applications, and research directions," *IEEE Communications Magazine*, vol. 59, no. 6, pp. 14–20, 2021.

[6] E. Björnson, Ö. Özdogan, and E. G. Larsson, "Reconfigurable intelligent surfaces: Three myths and two critical questions," *IEEE Commun. Mag.*, no. 12, pp. 90–96, 2020.

[7] L. Wei, C. Huang, G. C. Alexandropoulos, C. Yuen, Z. Zhang, and M. Debbah, "Channel estimation for ris-empowered multi-user miso wireless communications," *IEEE Transactions on Communications*, vol. 69, no. 6, pp. 4144–4157, 2021.

[8] E. Björnson and P. Ramezani, "Maximum likelihood channel estimation for RIS-aided communications with LOS channels," in *Asilomar Conference on Signals, Systems and Computers*, 2022.

[9] C. Huang, A. Zappone, G. C. Alexandropoulos, M. Debbah, and C. Yuen, "Reconfigurable intelligent surfaces for energy efficiency in wireless communication," *IEEE Trans. Commun.*, vol. 18, no. 8, pp. 4157–4170, 2019.

[10] G. Mylonopoulos, C. DAndrea, and S. Buzzi, "Active reconfigurable intelligent surfaces for user localization in mmWave MIMO systems," in *IEEE 23rd International Workshop on Signal Processing Advances in Wireless Communication (SPAWC)*, 2022, pp. 1–5.

[11] N. Garg, H. Ge, and T. Ratnarajah, "Generalized superimposed training scheme in irs-assisted cell-free massive mimo systems," *IEEE Journal of Selected Topics in Signal Processing*, vol. 16, no. 5, pp. 1157–1171, 2022.

[12] 3GPP, "NR; Physical channels and modulation," 3rd Generation Partnership Project (3GPP), Technical Specification (TS) 38.211, 09 2022, version 17.4.0.

[13] H. V. Poor, *An Introduction to Signal Detection and Estimation (2nd Ed.)*. Berlin, Heidelberg: Springer-Verlag, 1994.

[14] S. M. Kay, *Fundamentals of Statistical Signal Processing, Volume I: Estimation Theory*. Prentice Hall, 1993.